Tumor Biol. (2015) 36:3285–3291
DOI 10.1007/s13277-014-2958-x

RESEARCH ARTICLE

MicroPET imaging of tumor angiogenesis and monitoring on antiangiogenic therapy with an ^{18}F labeled RGD-based probe in SKOV-3 xenograft-bearing mice

Guangjie Yang · Pei Nie · Yu Kong · Hukui Sun · Guihua Hou · Jiankui Han

Received: 28 October 2014 / Accepted: 5 December 2014 / Published online: 13 December 2014

Abstract So far, there is no satisfactory imaging modality to monitor antiangiogenesis therapy of ovarian cancer noninvasively. The aim of this study was to evaluate the effectiveness and sensibility of an ^{18}F labeled Arg-Gly-Asp (RGD) peptide in imaging and monitoring antiangiogenic responds in SKOV-3 xenograft-bearing mice. ^{18}F-FB-NH-PEG$_4$-E[PEG$_4$-c(RGDfK)]$_2$ (denoted as ^{18}F-RGD$_2$) was synthesized and employed in this study. Mice bearing ovarian cancer SKOV-3 tumors were used for biodistribution and microPET imaging studies compared with ^{18}F-FDG imaging. Animals were treated with low-dose paclitaxel and the effect of paclitaxel therapy on ^{18}F-RGD$_2$ accumulation was investigated. Microvascular density (MVD) of SKOV-3 tumors was detected to assess the reliability of ^{18}F-RGD$_2$ in antiangiogenesis monitoring. Biodistribution studies for ^{18}F-RGD$_2$ revealed favorable in vivo pharmacokinetic properties, with significant levels of receptor-specific tumor uptake determined via blocking studies. MicroPET imaging results demonstrated high contrast visualization of SKOV-3 tumors. And tumor to background ratio (T/NT) of ^{18}F-RGD$_2$ uptake was significantly higher than that of ^{18}F-FDG. Studies on antiangiogenic therapy demonstrated percentage of injected dose per gram of tissue (%ID/g) tumor uptake of ^{18}F-RGD$_2$ which was obviously decreased in the treatment group than the control group, especially at 60 min (by 31.31±7.18 %, P=0.009) and 120 min (by 38.92±8.31 %, P<0.001) after injection of ^{18}F-RGD$_2$. MVD measurement of SKOV-3 tumors confirmed the finding of the biodistribution studies in monitoring antiangiogenesis therapy. ^{18}F-RGD$_2$, with favorable biodistribution properties and specific affinity, is a promising tracer for tumor imaging and monitoring antiangiogenesis therapy in ovarian cancer SKOV-3 xenograft-bearing mice.

Keywords Ovarian cancer · Monitoring antiangiogenic therapy · Target imaging · RGD peptide · Integrin imaging

Introduction

As the second most common gynecological malignancy worldwide, ovarian cancer is often not found until it is advanced or has spread [1]. It is generally considered sensitive to chemotherapy. Patients should be treated with optimal cytoreductive surgery combined with adjuvant carboplatin–paclitaxel chemotherapy, while some unresectable patients are treated with up-front chemotherapy [2]. Although the 5-year survival for women presenting with advanced ovarian cancer has shown some improvement for the past few years (to 40–50 %), most patients will still die of this disease [3]. A large number of trials have proven that antiangiogenic therapy plays an important role in the treatment of various stages of ovarian cancer [4–7].

Recently, some encouraging results of successful antiangiogenic therapy in combination with chemotherapy and radiotherapy in various carcinomas have been reported [8, 9]. Consequently, there is an increasing demand for noninvasive imaging to facilitate early response monitoring and

G. Yang · Y. Kong · J. Han (✉)
Department of Nuclear Medicine, Qilu Hospital, Shandong University, No.107 Wenhuaxi Road, Jinan, Shandong, China
e-mail: hanjiank@163.com

P. Nie
Department of Radiology, the Affiliated Hospital of Qingdao University, Qingdao, Shandong, China

H. Sun · G. Hou (✉)
Key Laboratory for Experimental Teratology of the Ministry of Education and Institute of Experimental Nuclear Medicine, School of Medicine, Shandong University, No. 44 Wenhuaxi Road, Jinan, Shandong 250012, China
e-mail: ghhou.1@hotmail.com

screening of the appropriate patients who will benefit from antiangiogenic treatment with positive effects [10, 11].

Integrin αvβ3 is expressed on tumor neovessels as well as on some tumor cells but not on quiescent blood vessels in normal tissue [12]. Due to the high integrin αvβ3-binding affinity, many RGD-target probes have been developed for multimodality imaging of integrin expression with the purpose of tumor diagnosis and monitoring tumor treatment response [13–15].

Paclitaxel is one of the most important first line anticancer drugs for ovarian cancer. But the mechanisms of its antitumor activity are not entirely understood. Various mechanisms of paclitaxel have been reported including cell cycle arrest, induction of apoptosis, and stabilization of microtubules. In addition, the recent studies indicate that inhibition of angiogenesis also plays an important role in its antitumor activity [16–18]. We had reported that paclitaxel therapy could inhibit tumor growth, proliferation, and angiogenesis in SKOV-3 xenografts [19]. And the results also demonstrated that paclitaxel therapy could decrease expression of integrin αvβ3 on tumor vascular endothelial cells due to the decrease of tumor microvascular density (MVD) but did not affect expression of integrin αvβ3 on SKOV-3 tumor cells, which indicate that imaging of integrin αvβ3 expression is suitable for antiangiogenic monitoring of paclitaxel therapy.

In the present study, we synthesized the ^{18}F labeled ^{18}F-FB-NH-PEG$_4$-E[PEG$_4$-c(RGDfK)]$_2$ (noted as ^{18}F-RGD$_2$), as a radiotracer on integrin αvβ3 imaging. And then the biodistribution of ^{18}F-RGD$_2$ was determined. Subsequently, the ability of ^{18}F-RGD$_2$ for imaging and antiangiogenesis monitoring of ovarian cancer was examined.

Materials and methods

Preparation of ^{18}F-RGD$_2$

E[c(RGDfK)]$_2$ and NH$_2$-PEG$_4$-E[PEG$_4$-c(RGDfK)]$_2$ (denoted as RGD$_2$) were custom-made by ChinaPeptides Co., Ltd. (Shanghai, China). *N*-Succinimidyl-4-^{18}F-fluorobenzoate (^{18}F-SFB) was synthesized as previously reported [20]. All other chemicals were acquired from Sigma-Aldrich. The ^{18}F-fluoride in O-18 water was obtained from a GE MINItrace Cyclotron (GE Healthcare, Buckinghamshire, UK).

The purified ^{18}F-SFB was rotary evaporated to dryness, redissolved in dimethyl sulfoxide (DMSO, 200 μl), and added to a DMSO solution of RGD$_2$ (1 mg, 0.5 μmol) and *N*,*N*-diisopropylethylamine (DIPEA, 30 μl). The reaction mixture was allowed to incubate at 60 °C for 30 min. After dilution with 1000 μl of water with 1 % trifluoroacetic acid (TFA), the mixture was diluted with 10 ml of water and the desired product trapped on a Sep-Pak C18 column (Waters Corporation, MA, USA). The column was washed with another 10 ml of water, and the radioactivity trapped on the C18 column was eluted with 0.3 ml of ethanol. The ethanol solution of ^{18}F-RGD$_2$ (Fig. 1) was diluted with PBS for further study, and the radiochemical purity was checked by the radio high-performance liquid chromatography (radio-HPLC).

HPLC was done in a Kromasil 100-5-C18 reverse phase column (4.6×250 mm, 100-Å pore size). The flow rate for HPLC was set at 1 ml/min from 90 % solvent A (0.1 % TFA in water) and 10 % solvent B (0.1 % TFA in acetonitrile) at 0–2 min, followed by a gradient mobile phase going from 10 % solvent B at 2 min to 50 % solvent B at 13 min.

The stability in vitro mouse serum of the labeled RGD peptide was tested for up to 2 h. About 5.0 MBq of radiolabeled RGD peptide was incubated with 200 μl of mouse serum at 37 °C. Samples of the sulution containing the radiotracer were analyzed with HPLC at 0, 15, 30, 60, and 120 min.

Preparation of tumor-bearing mice

The animal protocol was reviewed and approved by the Institutional Animal Care and Use Committee at School of Medicine, Shandong University.

The ovarian carcinoma cells SKOV-3 were purchased from ATCC (American Type Culture Collection, Manassas, VA, USA) and cultured in McCoy's 5a Medium (Invitrogen, Carlsbad, CA, USA), supplemented with 10 % fetal bovine serum (Gibco BRL, Gaithersburg, MD, USA). Cells were grown at 37 °C in an atmosphere of 5 % CO_2.

Female athymic nu/nu mice (Shanghai SLAC Laboratory Animal Co., Ltd, Shanghai, China) at 4 to 6 weeks of age were subcutaneously implanted with 5×10^6 SKOV-3 cells in 0.1 ml of saline into the left front flank. All procedures were performed in a laminar flow cabinet using aseptic techniques. The animals were allowed to feed ad libitum. Biodistribution studies were performed when the tumor volume reached about 50 mm^3 (8–10 days after implantation).

Biodistribution studies

Mice were injected with 1 MBq/0.1 ml ^{18}F-RGD$_2$ via tail vein and were humanely sacrificed at 30, 60, and 120 min after injection (n=4 per time point). Blood, tumor, major organs, and tissues were collected, weighed, and counted using a gamma-counter. The results were presented as percentage of injected dose per gram of tissue (%ID/g).

For the blocking experiment, E[c(RGDfK)]$_2$ was dissolved in the solution containing ^{18}F-RGD$_2$ to give a concentration of 3.5 mg/ml (excess, 14 mg/kg). SKOV-3 xenograft-bearing mice were injected with 0.1 ml of the above solution containing 1 MBq ^{18}F-RGD$_2$ along with unlabeled E[c(RGDfK)]$_2$. Mice were sacrificed at 60 min after injection for organ biodistribution using the same procedure above.

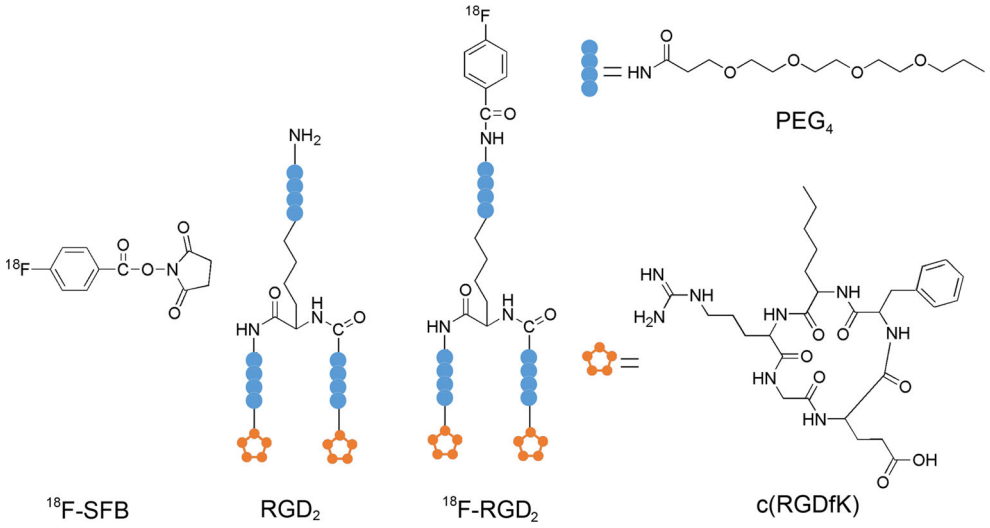

Fig. 1 Structural formulas of ^{18}F-SFB, RGD_2, and ^{18}F-RGD_2. ^{18}F-SFB=*N*-succinimidyl-4-^{18}F-fluorobenzoate; RGD_2=NH_2-PEG_4-E[PEG_4-c(RGDfK)]$_2$; ^{18}F-RGD_2=^{18}F-FB-NH-PEG_4-E[PEG_4-c(RGDfK)]$_2$

MicroPET imaging

The microPET static scans were performed using an Inveon microPET scanner (Siemens Medical Solutions). Two groups of animals were anesthetized with intraperitoneal injection of sodium pentobarbital at a dosage of 60 mg/kg body weight. Five-minute static scans were acquired at 60 min after injection of 3.7 MBq ^{18}F-RGD_2 or 5 MBq ^{18}F-FDG (n=6 per group). The images were reconstructed using a two-dimensional ordered-subset expectation maximization algorithm, and no correction was applied for attenuation or scatter. For each microPET scan, regions of interest (ROIs) were drawn over the tumor or muscle using vendor software ASI Pro 5.2.4.0 on decay-corrected whole-body coronal images. The maximum radioactivity concentrations (accumulation) were obtained from maximum pixel values within the multiple ROI volumes and then converted to MBq per milliliter per minute using a conversion factor. Uptake from the tumor was compared with the muscle, which was taken as background uptake and expressed as the tumor to background ratio (T/NT). Tumor size was determined by caliper measurements of perpendicular diameters of the tumors. The tumor volume was estimated by the formula tumor volume=$a\times b\times b/2$, where a and b were the tumor's greatest diameter and smallest diameter, respectively, in millimeters.

Paclitaxel therapy protocol

We utilized ovarian carcinoma mouse model to evaluate the ability of ^{18}F-RGD_2 in monitoring the therapeutic response of paclitaxel (Sigma-Aldrich, St. Louis, MO, USA). Paclitaxel were dissolved in dimethyl sulfoxide and diluted by PBS to specified concentrations before use. The final concentration of dimethyl sulfoxide in treated cultures was <0.1 %. For biodistribution studies, mice with ovarian cancer were divided into two groups by means of random number table (n=12 per group). The mice were treated according to one of the following conditions. Briefly, the mice were injected with 0.1 ml of paclitaxel at a dosage of 10 mg/kg body weight (treatment group) or with 0.1 ml of PBS (control group). Therapies were performed every 3 days for 16 days (six injections).

Detection of MVD on SKOV-3 tumor tissue

Immunohistochemical analysis of the SKOV-3 tumor tissues harvested from the eight mice was performed 1 day after the biodistribution studies at 120 min after injection. After histologic processing, 4-mm slices from SKOV-3 tumors were analyzed for MVD. MVD was evaluated by immunohistochemical analysis with antibodies to the endothelial marker CD34 and determined according to the method of Weidner [21]. Briefly, the immunostained sections were initially screened at low magnification (×40) to identify hot spots, which are the areas of highest neovascularization. Any yellow brown-stained endothelial cell or endothelial cell cluster that was clearly separate from adjacent microvessels, tumor cells, and other connective tissue elements was considered a single, countable microvessel. Within the hot spot area, the stained microvessels were counted in a single high-power field (×200), and the average vessel count in five hot spots was considered the value of MVD.

Data analysis

Quantitative data were expressed as mean±SD. Data was analyzed by t test with GraphPad statistical software (GraphPad Software Inc., San Diego, CA, USA). Differences were considered significant at P<0.05.

Results

Radiochemistry, serum stability, and biodistribution of ^{18}F-RGD$_2$

The radiochemical purity of product determined by radio-HPLC was 96.84±0.18 % (the retention time=9.091 min, three times repeated). The specific activity was approximately 31 GBq/μmol. To study the stability of ^{18}F-RGD$_2$, the peptide was incubated in mouse serum at 37 °C for up to 2 h and analyzed by radio-HPLC. The result showed that there was a high radiochemical purity even after incubation for 2 h (>92 %), indicating the excellent stability of the imaging tracer.

The results of biodistribution studies showed that ^{18}F-RGD$_2$ exhibited good imaging properties, with significantly higher tumor uptake than the background (Table 1 and Fig. 2). For example, tumor uptake measured by the gamma-counter was 2.13±0.19 %ID/g and the tumor to blood and muscle ratio was 7.1 and 4.7, respectively, at 60 min after injection of tracer. Co-injection of unlabeled dimeric RGD peptide effectively blocked tumor uptake.

MicroPET scans on the SKOV-3 tumors

The tumor volumes and whole body weights of mice were shown (Fig. 3a, b). MicroPET static imaging was performed at 60 min after injection of ^{18}F-RGD$_2$ compared with ^{18}F-FDG. ^{18}F-RGD$_2$ imaging of SKOV-3 tumors, with high tumor/muscle contrast, were more visible than ^{18}F-FDG imaging (Fig. 3c). Quantification of T/NT ratio of ^{18}F-RGD$_2$ imaging and ^{18}F-RGD imaging (6.04±0.92 and 3.34±0.79, respectively, $P<0.05$) agreed well with the characteristic of microPET imagings (Fig. 3d). The microPET imagings were also in good agreement with the data from biodistribution studies.

Table 1 Biodistribution of ^{18}F-RGD$_2$ in SKOV-3 xenograft-bearing mice

	30 min	60 min	120 min	Blocking
Blood	0.45±0.04	0.30±0.02	0.11±0.01	0.23±0.01
Muscle	0.57±0.02	0.45±0.01	0.13±0.02	0.25±0.02
Bone	0.55±0.11	0.42±0.04	0.20±0.05	0.25±0.01
Brain	1.28±0.14	1.08±0.15	0.78±0.06	0.68±0.08
Heart	1.67±0.16	1.37±0.12	0.82±0.11	0.89±0.17
Liver	2.72±0.44	2.27±0.49	1.77±0.39	1.17±0.34
Lungs	1.14±0.15	0.89±0.11	0.54±0.13	0.47±0.09
Kidney	4.96±0.55	3.98±0.63	2.08±0.31	2.25±0.45
Intestines	1.98±0.34	1.58±0.38	1.09±0.27	0.79±0.08
Tumor	2.15±0.14	2.13±0.19	1.92±0.09	0.24±0.04

Data shown as %ID/g. %ID/g=percentage of injected dose per gram of tissue

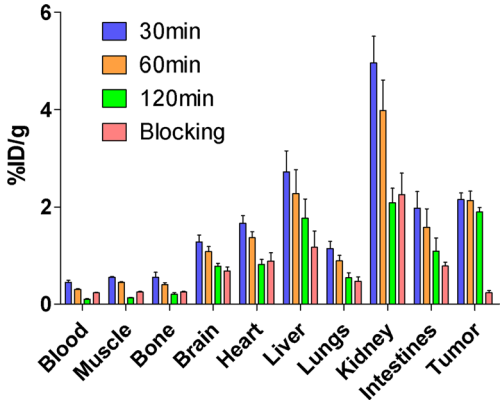

Fig. 2 Biodistribution of ^{18}F-RGD$_2$ in SKOV-3 xenograft-bearing nude mice. Each mouse was injected with 1 MBq of ^{18}F-RGD$_2$ and biodistribution was studied at 30, 60, and 120 min after injection with unlabeled RGD peptide as blocking agent at 60 min after injection. %ID/g=percentage of injected dose per gram of tissue

Effects of paclitaxel therapy on ^{18}F-RGD$_2$ accumulation and MVD in SKOV-3 tumors

This part of biodistribution studies were performed to investigate the ability of ^{18}F-RGD$_2$ in monitoring the antiangiogenic effect of paclitaxel. In the treatment group, tumor uptake showed a significant decrease compared with the control group at 30 min (by 6.45±1.24 %, $P=0.085$), 60 min (by 31.31±7.18 %, $P=0.009$), and 120 min (by 38.92±8.31 %, $P<0.001$) after injection of ^{18}F-RGD$_2$ (Fig. 4d). Especially, there was a significant difference at 60 and 120 min after injection (both $P<0.05$).

To corroborate the reliability of ^{18}F-RGD$_2$ in monitoring antiangiogenesis in the above biodistribution studies, tumor angiogenesis was evaluated by CD34 immunohistochemical staining (Fig. 4a). CD34 expression markedly decreased in the paclitaxel-treated group compared with the control group (Fig. 4b, by 39.1±5.8 %, $P<0.05$). Similar to CD34 expression, paclitaxel treatment led to a 48 % reduction in MVD levels (Fig. 4c).

Discussion

Recently, more and more antiangiogenic agents were used in clinic in diverse types of carcinomas. Despite the initial promising performance of antiangiogenic agents, three major challenges are faced in the use of antiangiogenesis therapy, including inherent/acquired resistance, enhanced invasiveness during treatment, and lack of validated predictive biomarkers for monitoring tumors responses to the therapy [22]. Imaging of integrin $\alpha v\beta 3$ expression may be a possible solution to the third problem. In the preclinical researches, all sorts of imaging modalities have been successfully applied for imaging of

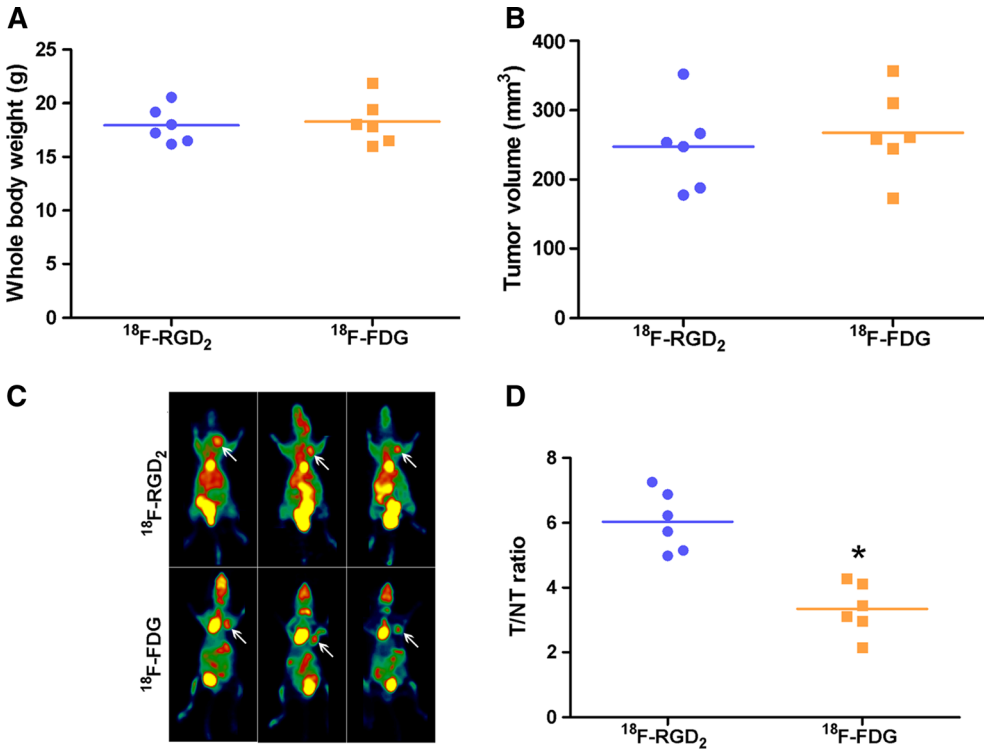

Fig. 3 In vivo microPET images of ^{18}F-RGD$_2$ and ^{18}F-FDG. **a**, **b** The tumor volumes and whole body weights of mice for microPET imaging. **c** Representative images of SKOV-3 xenograft-bearing mice after injection of 3.7 MBq of ^{18}F-RGD$_2$ (*upper panel*) or 5 MBq of ^{18}F-FDG (*lower panel*). *White arrow* shows SKOV-3 tumor. **d** Quantification of the tumor to background ratio (T/NT) of tracers uptake at 60 min after injection of ^{18}F-RGD$_2$ and ^{18}F-FDG (n=6 per group). *P<0.05 versus ^{18}F-RGD$_2$

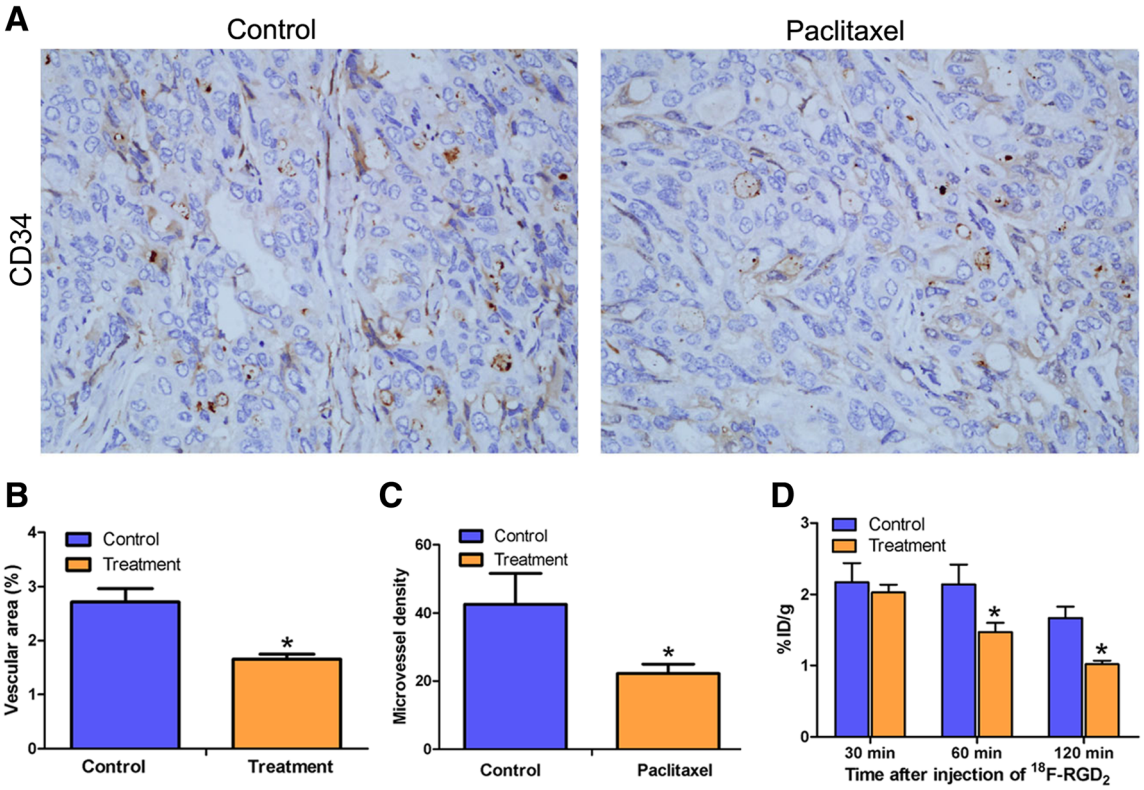

Fig. 4 Effects of paclitaxel therapy on angiogenesis and ^{18}F-RGD$_2$ accumulation in SKOV-3 xenograft-bearing nude mice. **a** Illustration of CD34 immunohistochemical detection in representative SKOV-3 tumor comparison with control group (images at 40 magnification). **b** Quantitative analysis of the percentage of CD34 expression. **c** Quantitative evaluation of microvessel density (MVD) by quantitating CD34-expressing vessels from hotspot areas, as described in "Materials and methods." **d** Quantitative analysis of paclitaxel therapy on ^{18}F-RGD$_2$ accumulation in vivo after injection of 1 MBq of ^{18}F-RGD$_2$ at 30, 60, and 120 min after injection. *P<0.05 versus control group. %ID/g= percentage of injected dose per gram of tissue

integrin expression, including PET or SPECT, MRI, targeted US, and optical imaging [23]. Radiolabeled techniques have the advantage over other modalities owing to their high sensitivity, and so far, only the use of RGD radiotracers has been successfully translated into clinic [24]. Several labeled monomeric or dimeric RGD peptides tracers had been investigated to monitor antiangiogenesis therapy efficacy in recent studies [25–27]. No clinical data regarding monitoring antiangiogenesis therapies is available on this subject yet, though some clinical trials have been completed [28, 29] and the others are ongoing [30–32].

In this study, we evaluated the ^{18}F labeled RGD peptide in imaging and therapy monitoring ovarian cancer. Biodistribution and blocking studies for ^{18}F-RGD$_2$ revealed favorable in vivo pharmacokinetic properties, with significant levels of receptor-specific tumor uptake. MicroPET imaging studies demonstrated high contrast visualization of SKOV-3 tumors. The kidneys showed the highest radioactivity accumulation in biodistribution studies, indicating dominant renal-urinary clearance of the imaging tracers. MicroPET imaging also confirmed this finding, with high activity in the bladder, indicating that ^{18}F-RGD$_2$ is excreted mainly via the kidneys into the urine. All the above results suggested ^{18}F-RGD$_2$ was a promising probe for tumor imaging and can be used in selecting patient population for antiangiogenesis therapy.

Although many kinds of RGD radiotracers were developed for the purpose of imaging integrin αvβ3, relatively little studies were focused on the ability of these radiotracers to monitor the response of tumors to therapies that target the vasculature, the most likely clinical use of these imaging agents. Jung et al. [25] stated that radiolabeled RGD peptide can be used for monitoring response to antiangiogenic therapy by demonstrating that paclitaxel therapy resulted in a decreased LLC uptake of a 99mTc-labeled glucosamino RGD-containing peptide. And it was reported that paclitaxel could cause an antiangiogenic effect at a low dose without significant tumor shrinkage [16]. In this study, the data suggested ^{18}F-RGD$_2$ could sensitively and reliably detect the antiangiogenic effect even under the low dose of paclitaxel. Higher T/NT ratio of ^{18}F-RGD$_2$ uptake means it is more sensitive for non-invasive tumor imaging than ^{18}F-FDG imaging, which is widely used in clinic.

In conclusion, the results presented in this article suggest that ^{18}F-RGD$_2$, with favorable biodistribution and imaging properties, is a promising tracer for tumor imaging and monitoring antiangiogenesis therapy in ovarian cancer SKOV-3 xenograft-bearing mice. And in the future, the radiotracer may be used in combination with other imaging modalities, which would reinforce our insight into the antiangiogenic mechanism of antiangiogenic agents.

Acknowledgments This work was supported by grants from the National Natural Science Foundation of China No. 81071172. The authors would like to thank Nanjing PET-Tracer Co., Ltd (Nanjing, Jiangsu, China) for the assistance with radiosynthesis of ^{18}F-RGD$_2$.

References

1. Ferlay J, Soerjomataram I, Ervik M, Forman D, Bray F. GLOBOCAN, GLOBOCAN. Cancer incidence and mortality worldwide; 2012. http://globocan.iarc.fr.
2. Syrios J, Banerjee S, Kaye SB. Advanced epithelial ovarian cancer: from standard chemotherapy to promising molecular pathway targets—where are we now? Anticancer Res. 2014;34:2069–77.
3. Howlader N, Noone AM, Krapcho M, Garshell J, Neyman N. SEER Cancer Statistics Review, 1975–2010, National Cancer Institute. Bethesda, MD, 2014; http://seer.cancer.gov/csr/1975_2010/.
4. PPerren TJ, Swart AM, Pfisterer J, Ledermann JA, Pujade-Lauraine E, Kristensen G, et al. A phase III trial of bevacizumab in ovarian cancer. N Engl J Med. 2011;365:2484–96.
5. Burger RA, Brady MF, Bookman MA, Fleming GF, Monk BJ, Huang H, et al. Incorporation of bevacizumab in the primary treatment of ovarian cancer. N Engl J Med. 2011;365:2473–83.
6. Kumar R, Knick VB, Rudolph SK, Johnson JH, Crosby RM, Crouthamel MC, et al. Pharmacokinetic-pharmacodynamic correlation from mouse to human with pazopanib, a multikinase angiogenesis inhibitor with potent antitumor and antiangiogenic activity. Mol Cancer Ther. 2007;6:2012–21.
7. Aghajanian C, Blank SV, Goff BA, Judson PL, Teneriello MG, Husain A, et al. OCEANS: a randomized, double-blind, placebo-controlled phase III trial of chemotherapy with or without bevacizumab in patients with platinum-sensitive recurrent epithelial ovarian, primary peritoneal, or fallopian tube cancer. J Clin Oncol. 2012;30:2039–45.
8. Chauhan VP, Stylianopoulos T, Martin JD, Popović Z, Chen O, Kamoun WS, et al. Normalization of tumour blood vessels improves the delivery of nanomedicines in a size-dependent manner. Nat Nanotechnol. 2012;7:383–8.
9. Beer AJ, Kessler H, Wester HJ, Schwaiger M. PET imaging of integrin αvβ3 expression. Theranostics. 2011;1:48–57.
10. Haubner R, Wester HJ. Radiolabeled tracers for imaging of tumor angiogenesis and evaluation of anti-angiogenic therapies. Curr Pharm Des. 2004;10:1439–55.
11. Mittra ES, Goris ML, Iagaru AH, Kardan A, Burton L, Berganos R, et al. Pilot pharmacokinetic and dosimetric studies of ^{18}F-FPPRGD2: a PET radiopharmaceutical agent for imaging αvβ3 integrin levels. Radiology. 2011;260:182–91.
12. Brooks PC, Montgomery AM, Rosenfeld M, Reisfeld RA, Hu T, Klier G, et al. Integrin alpha v beta 3 antagonists promote tumor regression by inducing apoptosis of angiogenic blood vessels. Cell. 1994;79:1157–64.
13. Moncelet D, Bouchaud V, Mellet P, Ribot E, Miraux S, Franconi JM, et al. Cellular density effect on RGD ligand internalization in glioblastoma for MRI application. PLoS One. 2012;8:e82777.
14. Metz S, Ganter C, Lorenzen S, van Marwick S, Herrmann K, Lordick F, et al. Phenotyping of tumor biology in patients by multimodality multiparametric imaging: relationship of microcirculation, alphavbeta3 expression, and glucose metabolism. J Nucl Med. 2010;51:1691–8.
15. HHaubner R, Weber WA, Beer AJ, Vabuliene E, Reim D, Sarbia M, et al. Noninvasive visualization of the activated alphavbeta3 integrin

in cancer patients by positron emission tomography and [^{18}F]Galacto-RGD. PLoS Med. 2005;2:e70.
16. Lau DH, Xue L, Young LJ, Burke PA, Cheung AT. Paclitaxel (Taxol): an inhibitor of angiogenesis in a highly vascularized transgenic breast cancer. Cancer Biother Radiopharm. 1999;14:31–6.
17. Merchan JR, Jayaram DR, Supko JG, He X, Bubley GJ, Sukhatme VP. Increased endothelial uptake of paclitaxel as a potential mechanism for its antiangiogenic effects: potentiation by Cox-2 inhibition. Int J Cancer. 2005;113:490–8.
18. Pasquier E, Carré M, Pourroy B, Camoin L, Rebaï O, Briand C, et al. Antiangiogenic activity of paclitaxel is associated with its cytostatic effect, mediated by the initiation but not completion of a mitochondrial apoptotic signaling pathway. Mol Cancer Ther. 2004;3:1301–10.
19. Yang G, Sun H, Kong Y, Hou G, Han J. Diversity of RGD radiotracers in monitoring antiangiogenesis of flavopiridol and paclitaxel in ovarian cancer xenograft-bearing mice. Nucl Med Biol. 2014;41:856–62.
20. Cai W, Olafsen T, Zhang X, Cao Q, Gambhir SS, Williams LE, et al. PET imaging of colorectal cancer in xenograft-bearing mice by use of an ^{18}F-labeled T84.66 anti-carcinoembryonic antigen diabody. J Nucl Med. 2007;48:304–10.
21. Weidner N, Semple JP, Welch WR, Folkman J. Tumor angiogenesis and metastasis: correlation in invasive breast carcinoma. N Engl J Med. 1991;324:1–8.
22. Shojaei F. Anti-angiogenesis therapy in cancer: current challenges and future perspectives. Cancer Lett. 2012;320:130–7.
23. Cai W, Chen X. Multimodality molecular imaging of tumor angiogenesis. J Nucl Med. 2008;49 Suppl 2:113–28.
24. Gaertner FC, Kessler H, Wester HJ, Schwaiger M, Beer AJ. RGD radiotracers for imaging and therapy. Eur J Nucl Med Mol Imaging. 2012;39 Suppl 1:126–38.
25. Jung KH, Lee KH, Paik JY, Ko BH, Bae JS, Lee BC, et al. Favorable biokinetic and tumor-targeting properties of 99mTc-labeled glucosamino RGD and effect of paclitaxel therapy. J Nucl Med. 2006;47:2000–7.
26. Dumont RA, Hildebrandt I, Su H, Haubner R, Reischl G, Czernin JG, et al. Noninvasive imaging of alphaVbeta3 function as a predictor of the antimigratory and antiproliferative effects of dasatinib. Cancer Res. 2009;69:3173–9.
27. Jin ZH, Furukawa T, Claron M, Boturyn D, Coll JL, Fukumura T, et al. Positron emission tomography imaging of tumor angiogenesis and monitoring of antiangiogenic efficacy using the novel tetrameric peptide probe 64Cu-cyclam-RAFT-c(−RGDfK-)4. Angiogenesis. 2012;15:569–80.
28. Aten E. Efficacy study of [F-18]RGD-K5 positron emission tomography (PET) as a tool to monitor response to an anti-angiogenic drug (K5-101). ClinicalTrials.gov; 2009.
29. Winick J. A proof-of-concept study to assess the ability of [^{18}F]AH-111585 PET imaging to detect tumours and angiogenesis. ClinicalTrials.gov; 2007.
30. Kyung Moon W. PET-MR for prediction and monitoring of response to neoadjuvant chemotherapy in breast cancer. ClinicalTrials.gov; 2010.
31. Gleeson F. RGD-PET-CT in cancer angiogenesis. ClinicalTrials.gov; 2011.
32. Gambhir S. ^{18}F FPPRGD2 positron emission tomography/computed tomography in predicting early response in patients with cancer receiving anti-angiogenesis therapy. ClinicalTrials.gov; 2013.